Tropical Cyclone Flooding in the Carolinas

MAOFENG LIU,[a] JAMES A. SMITH,[b] LONG YANG,[c] AND GABRIEL A. VECCHI[d,e]

[a] *Rosenstiel School of Marine and Atmospheric Science, University of Miami, Miami, Florida*
[b] *Department of Civil and Environmental Engineering, Princeton University, Princeton, New Jersey*
[c] *School of Geography and Ocean Science, Nanjing University, Nanjing, China*
[d] *Department of Geosciences, Princeton University, Princeton, New Jersey*
[e] *High Meadows Environmental Institute, Princeton University, Princeton, New Jersey*

(Manuscript received 13 June 2021, in final form 23 September 2021)

ABSTRACT: The climatology of tropical cyclone flooding in the Carolinas is analyzed through annual flood peak observations from 411 U.S. Geological Survey (USGS) stream gauging stations. Tropical cyclones (TCs) account for 28% of the top 10 annual flood peaks, 55% of record floods, and 91% of floods with peak magnitudes at least 5 times greater than the 10-yr floods, highlighting the prominent role of TCs for flood extremes in the Carolinas. Of all TC-related flood events, the top 10 storms account for nearly 1/3 of annual flood peaks and more than 2/3 of record floods, reflecting the dominant role of a small number of storms in determining the upper tail of flood peak distributions. Analyses of the 10 storms highlight both common elements and diversity in storm properties that are responsible for flood peaks. Extratropical transition and orographic enhancement are important elements of extreme TC flooding in the Carolinas. Analyses of the Great Flood of 1916 highlight the flood peak of 3115 $m^3 s^{-1}$ in French Broad River at Asheville, 2.6 times greater than the second-largest peak from a record of 124 years. We also examine the hydroclimatology, hydrometeorology, and hydrology of flooding from Hurricanes Matthew (2016) and Florence (2018). Results point to contrasting storm properties for the two events, including tracks as well as rainfall distribution and associated physical mechanisms. Climatological analyses of vertically integrated water vapor transport (IVT) highlight the critical role of anomalous moisture transport from the Atlantic Ocean in producing extreme rainfall and flooding over the Carolinas.

KEYWORDS: Extratropical transition, Flood events, Hurricanes/typhoons; Rainfall

1. Introduction

We have examined tropical cyclone (TC) flooding in the Carolinas (North Carolina and South Carolina) based on analyses of U.S. Geological Survey (USGS) stream gauging records and hydrometeorological analyses of storm properties. The primary objective of this study is to provide improved characterizations of extreme rainfall and flood hazards associated with TCs. The Carolinas have substantial exposure to TC-induced hazards, with coastal areas exposed to surge, and both coastal and inland areas exposed to freshwater flooding and wind damage. The mean annual count of TCs in the Carolinas exceeds one, given an impact radius of 200 km, but with large temporal variability (Konrad and Perry 2010).

TCs are a substantial contributor to rainfall in the Carolinas. Knight and Davis (2007) found that TCs were responsible for as much as 15% of total rainfall in the hurricane season (June–November) in portions of the Carolinas through analyses of rain gauge observations over the period of 1980–2004. Prat and Nelson (2012) found a greater contribution (15%–20%) in the hurricane season in the coasts of Carolinas during the period of 1998–2009. For peak hurricane months (September–November), the contribution of TCs to rainfall in the Carolinas reached 20%–25% over the period of 1970–2014 based on a dense rain gauge network (Khouakhi et al. 2016).

In the Carolinas, TCs play an even more prominent role in rainfall extremes than for seasonal rainfall. Analyses of 55 years of daily rainfall observations found that more than 40% of rainfall events with at least 5-yr recurrence interval were associated with TCs in the western Carolinas, with the fraction increased to up to 90% in the eastern Carolinas (Konrad and Perry 2010). For rainfall events with 24-h accumulations exceeding 2 in. (50.8 mm), TCs accounted for approximately 20% (Knight and Davis 2009), which increased to 33%–67% or greater for rainfall days with accumulations above 4 in. (101.6 mm) (Barlow 2011). The results highlight the increasingly prominent role of TCs toward greater rainfall extremes. For rainfall extremes at hourly scales, the contribution of TCs to rainfall rate exceeding 20 mm h^{-1} reached 20% in the southeastern United States (Prat and Nelson 2012). Differences in values reported in these studies can be attributed to definitions of rainfall extremes, data sources, and study periods (Khouakhi et al. 2016).

The studies noted above provide a backdrop for understanding the role of TCs in flooding in the Carolinas, but inferences about flooding cannot be made directly from rain because other factors (including land cover, river network structure, and antecedent soil moisture conditions) can be crucial in determining flood response (e.g., Chen et al. 2015). Paerl et al. (2019) suggested there has been a temporal regime shift of TC flooding in coastal North Carolina based on long records from a rain gauge and a stream gauging station. To provide a more comprehensive view, the present study examines the TC flood climatology in the Carolinas through a comprehensive examination of USGS flood records.

Corresponding author: Maofeng Liu, maofengliu2012@gmail.com

DOI: 10.1175/JHM-D-21-0113.1

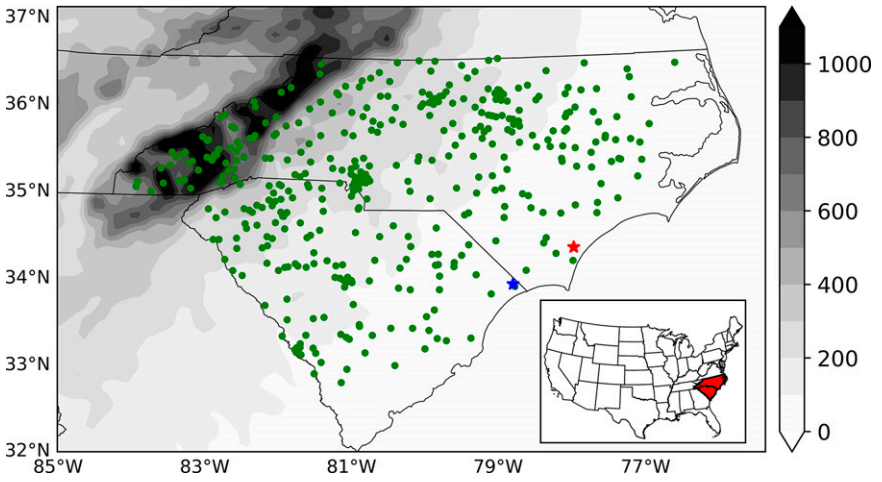

FIG. 1. Locations of stream gauging stations (green circles) in the Carolinas. The star symbols indicate the two GPS sites: red for the NCCH site and blue for the SCHY site. The gray shading indicates the topography (m). Locations of the Carolinas are indicated in red shading in the lower right subfigure.

Analyses of flood hydroclimatology highlight the challenge of projecting TC flood hazard under a future climate (e.g., Liu et al. 2018, 2019; Yang et al. 2020). Another important motivation of this study arises from the two recent hurricanes that caused devastating damages in the Carolinas: Matthew in 2016 and Florence in 2018. For North Carolina alone, Matthew caused approximately $4.5 billion in economic loss, while Florence surpassed that with $17 billion. A primary cause of the devastating damages is flooding; the two storms produced catastrophic flooding that set new records in a variety of river basins in the Carolinas although they exhibited large contrasts in storm properties (see section 4 for details). By placing Florence in historical context, Kunkel and Champion (2019) found Florence was the seventh largest event in the conterminous United States over a period of 1949–2018 in terms of 4-day precipitation over an area of 50 000 km^2.

In this study, we use USGS stream gauging records as key resources to examine the climatology of TC flooding in the Carolinas. A crucial step is to compare TCs with other flood agents for improved understanding of mixture of flood-generating mechanisms (Smith et al. 2018; Villarini and Smith 2010). We focus on TCs that produced the most "extreme" flooding by examining the contribution of these storms to flooding. Analyses of storm properties are conducted to shed light on nature of storms that produce extreme flooding. The "Great Flood of 1916" that was caused by two consecutive hurricanes produced arguably the worst flooding in western North Carolina. We examine the historic flood event by placing it in a climatological context.

Our analyses of Hurricane Matthew (2016) and Florence (2018) focus on the hydrometeorological and hydrologic processes responsible for extreme flooding of the two events. A detailed examination of rainfall evolution highlights the need for improved TC rainfall forecasts that serve the need for effective TC flood hazard adaption. By providing details of regional-scale flood response, our analyses can 1) facilitate a predictive understanding of TC flooding and 2) highlight the need for additional strategies of improved TC rainfall monitoring and forecasts. An important element of the analyses concerns contrasting storm properties of the two hurricanes.

The paper is organized as follows. In section 2 we present data and method. Section 3 shows results on climatology of TC flooding, followed by analyses of Matthew and Florence in section 4. A summary and conclusions are presented in section 5.

2. Data and methods

We use instantaneous annual maximum peak discharge data from 411 USGS stream gauging stations with a record of at least 20 years during the period of 1930–2018 (Fig. 1). The peak discharge data are used to examine the climatology of TC flooding in the Carolinas. Instantaneous 15-min discharge observations for Trent River near Trenton in North Carolina are used to examine the hydrology of flooding associated with Hurricane Florence (2018).

The best track data from the Atlantic hurricane database (HURDAT2; Landsea and Franklin 2013) of National Hurricane Center are used to examine storm properties (e.g., track and intensity) of historical TCs. We link a TC to an annual flood peak from a stream gauging station if the station is within 500 km (e.g., Chavas and Emanuel 2010; Jiang and Zipser 2010; Khouakhi et al. 2016; Liu et al. 2018; Smith et al. 2010; Villarini et al. 2014; Villarini and Smith 2010; Wright et al. 2015) from the circulation center of the storm during a time window of two days prior to and seven days after the passage of the storm (e.g., Villarini et al. 2014; Villarini and Smith 2010). Since the best-track data follow the storm center and the impact of TC rainfall extends well beyond

TABLE 1. Flood summary in the Carolinas based on 411 stream gauging stations over the period of 1930–2018, including counts of all flood events, flood events produced by tropical cyclones, and the fraction of flood events that were caused by TC flood events for a variety of flood metrics.

Metrics	All flood events (No.)	TC flood events (No.)	Fraction of TC floods (%)
Annual flood peak	18 478	2874	16
Top 10 flood peak	4110	1195	28
Record flood	411	227	55
Flood ratio ≥ 1	1899	737	39
Flood ratio ≥ 5	22	20	91

the center of the storm, we define TC landfall as occurring when the circulation center of a given storm is within 500 km from the Carolina coastline.

We use a variety of flood metrics to represent the varying magnitudes of flood peaks produced by TCs. For each station, record flood is the largest flood peak the station has ever recorded. We also use the 10 largest flood peaks from each station and calculate the fraction produced by TCs. Flood ratio is defined as the ratio of a flood peak produced by a TC to at-site sample 10-yr flood peak that corresponds to the 90th percentile of flood peak distribution (Aryal et al. 2018; Smith et al. 2018; Villarini et al. 2014). The notion of flood ratio diminishes the impact of drainage area on flood peaks to enable a regional view of the influence of TCs on the upper tail properties of flood distributions (see also Yang et al. 2020).

We examined the temporal and spatial evolution of rainfall fields from Matthew and Florence using Stage IV multisensor rainfall product. Stage IV is generated by National Oceanic and Atmospheric Administration (NOAA) National Centers for Environmental Prediction (NCEP) and provides rainfall fields with hourly interval at a ~4-km resolution (Lin and Mitchell 2005). Stage IV has been used for examining storm total rainfall accumulations (e.g., Jiang et al. 2008b; Marchok et al. 2007) and spatial and temporal evolution of rainfall fields (e.g., Liu and Smith 2016; Villarini et al. 2011) for landfalling TCs.

The Twentieth Century Reanalysis with 6-hourly fields (Compo et al. 2015) was used to examine anomalies of vertically integrated water vapor fluxes from two hurricanes that produced the Great Flood of 1916 relative to the period of 1910–2014. Similarly, the Japanese 55-year Reanalysis with 6-hourly fields (JRA-55; Kobayashi et al. 2015) was used to examine anomalies of vertically integrated water vapor fluxes from Matthew and Florence relative to the period of 1958–2018.

Measurements of column integrated precipitable water (PW) at two sites from the SuomiNet Global Positioning System (GPS) network (Ware et al. 2000) were used to examine PW for Florence (Fig. 1). PW from a downscaling simulation based on the Weather Research Forecasting (WRF) Model version 3.6 (Skamarock et al. 2008) was also used to compare with GPS measurements. The NCEP FNL (Final) Operational Global Analysis data analysis fields are used for initial and boundary conditions of the WRF simulation.

3. Climatology of tropical cyclone flooding in the Carolinas

a. Temporal and spatial characteristics

TCs are key flood agents in the Carolinas. There are 162 TCs that produced at least one annual flood peak over the period of 1930–2018, translating to a return period of 0.6 years. The return period increases to 1.1 years for 10-yr flood peaks and 2.4 years for record floods, highlighting severe flood hazards associated with TCs in the two states.

TCs are responsible for 16% of observed annual flood peaks from 411 stream gauging stations (Table 1). This percentage increases to 28% for the 10 largest flood peaks, 55% (227/411) for record floods, and 39% and 91% (20/22) for flood peaks with flood ratio larger than 1 and 5, respectively (Table 1). The results highlight the increasingly prominent role of TCs in representing the upper tail of flood peak distributions rather than the central portion, reflecting the nature of mixture distributions of flooding in the Carolinas (Smith et al. 2010).

We examined interannual variability and long-term trends in flood peaks produced by TCs using 94 stream gauging stations with a continuous flood record during the period from 1950 to 2018. There is large variability in counts of TCs making landfall in the Carolinas, ranging from one to nine (Fig. 2a). The counts would decrease if we narrowed the definition of landfall to storms with circulation centers passing over coastal lines. The large variability is also seen in the annual counts of TCs that produced at least one flood peak (Fig. 2b) and counts of annual and 10-yr flood events (Figs. 2c,d). Temporal clustering of TCs in the Atlantic (e.g., Mumby et al. 2011; Tippett et al. 2010; Vecchi et al. 2011, 2014; Villarini et al. 2010) and landfall ratio (e.g., Murakami et al. 2016; Villarini et al. 2012) are both important in modulating interannual variability of landfalling TCs. The variability of flood events associated with TCs also involves physical processes modulating storm rainfall fields (e.g., Chen et al. 2006; Houze 2010).

We find no significant evidence of long-term trends in landfalling storm frequency based on the ordinary least squares regression (Fig. 2a; $p = 0.95$ based on a two-sided t test). Annual counts of TCs that produced at least one flood peak, however, exhibit an upward trend but with little statistical significance (Fig. 2b; $p = 0.26$). There is also an increasing long-term trend in annual counts of annual and 10-yr flood events (Figs. 2c,d), with marginal significance ($p = 0.20$ and 0.16, respectively). Based on analyses of individual rain gauges and

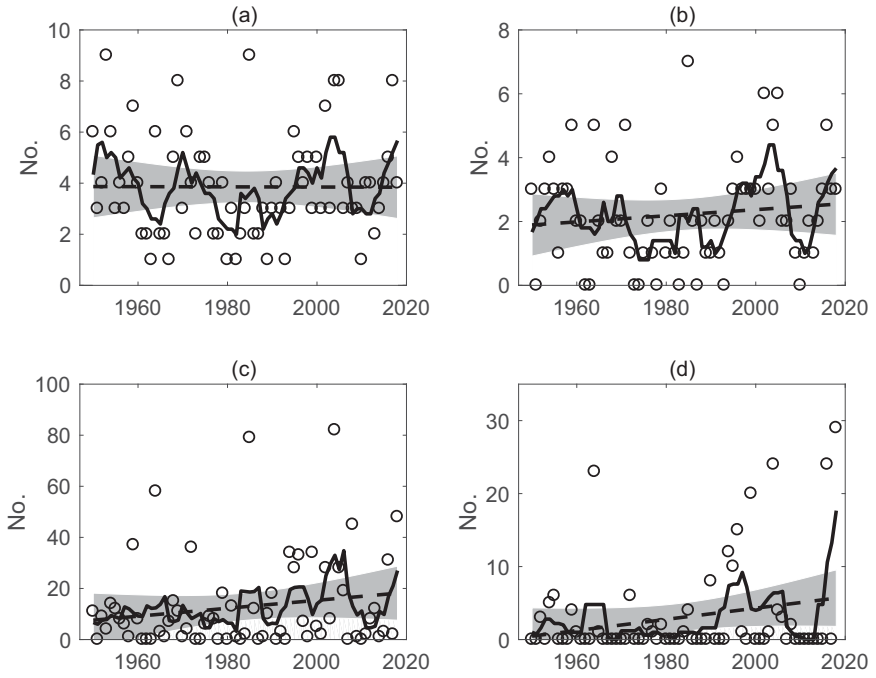

FIG. 2. Time series of annual frequency (open circles) of (a) landfalling tropical cyclones, (b) tropical cyclones that caused at least one annual flood peak, (c) annual flood peaks, and (d) 10-yr flood peaks (i.e., flood ratio ≥ 1) produced by tropical cyclones in the Carolinas. Solid black lines indicate the 5-yr moving average. Dashed black lines indicate linear trends based on ordinary least squares regression. The gray shadings indicate two-sided 95% confidence bounds of the trends. The p values for the four regressions based on the t test are 0.95, 0.26, 0.20 and 0.16, respectively. To avoid concerns over the skewness of distributions due to a lower bound of zero, the t test was performed over the time series of the square root of the original data series.

a stream gauging station with a record of over 100 years, Paerl et al. (2019) suggested a regime shift of TC flooding in coastal North Carolina due to recent high precipitation events from TCs. Our analyses include more stream gauging stations and show a consistently increasing long-term trend of flood peaks associated with TCs, but with marginal statistical significance, reflecting complex interplay between clustering properties of landfalling TCs, storm rainfall fields, and river networks.

The spatial distribution of record floods highlights the role of extreme rainfall from TCs in producing extreme floods in inland areas (Fig. 3), different from storm surge for which the impact is restricted within coastal areas (e.g., Marsooli et al. 2019). Record floods produced by TCs do not show spatial clustering that is fundamentally distinct from other flood-generating systems (Fig. 3). The map of flood ratio exhibits large spatial heterogeneity, reflecting complex interactions between river networks and spatially and temporally varying rainfall fields from TCs (Fig. 3). Difference in record length among stations is another contributing factor to the spatial heterogeneity (Smith et al. 2018). An important element of the spatial heterogeneity is associated with mountainous terrain (e.g., Liu et al. 2018; Liu and Smith 2016; Smith et al. 2010), as illustrated by large flood ratios in regions along the western boundary of North Carolina (i.e., the windward side of the eastern margin of the Blue Ridge Mountains; Fig. 1). In the Carolinas, there are two flood events with a peak that is 10 times greater than the 10-yr flood peak, and they were both produced by TCs: 12.6 in Trent River near Trenton, North Carolina (drainage area of 435 km^2; USGS ID 02092500), by Florence in 2018 (see section 4 for details) and 12.2 in Yadkin River at Wilkesboro, North Carolina (drainage area of 1305 km^2; USGS ID 02112000), by the 1940 South Carolina Hurricane, highlighting the crucial role of TCs in the upper tail of flood peak distribution (Smith et al. 2010, 2018; Villarini and Smith 2010).

We examined the spatial distribution of the fraction of the 10 largest and annual flood peaks that are caused by TCs (Fig. 4). Similar to the flood ratio map for record floods (Fig. 3), the fraction map for the 10 largest and annual flood peaks also exhibits large spatial heterogeneity (Fig. 4). For 75 of the 411 stations, TCs are responsible for at least half of the 10 largest flood peaks (Villarini and Smith 2010). TCs play a lesser role in the lower portion of flood peak distribution: compared to the 10 largest flood peaks (Fig. 4a), a smaller fraction of annual flood peaks is produced by TCs (Fig. 4b).

b. *Top 10 tropical cyclones*

A key feature of TC flooding in the Carolinas is the role of a small number of storms in accounting for the bulk of the

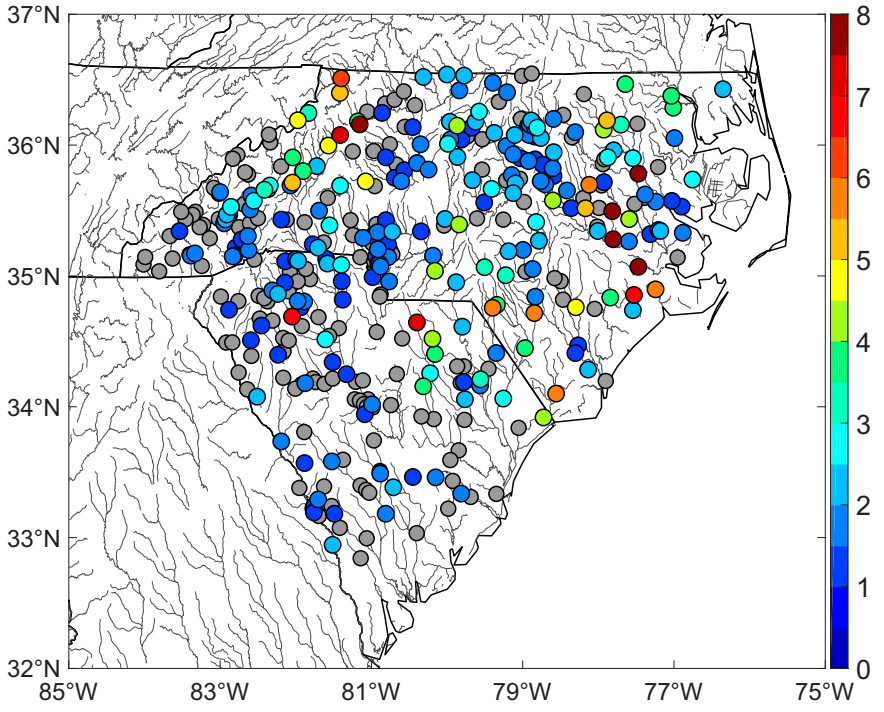

FIG. 3. Map showing flood ratio (i.e., Q_{TC}/Q_{10}) of stream gauging stations with record flood caused by tropical cyclones. The gray circles show stations with record flood produced by flood-generating systems rather than tropical cyclones.

flood hazards. We ranked storms in order based on the counts of 10-yr flood peaks and picked top 10 TCs from the list for further analyses (Table 2). The 1940 South Carolina Storm produced the largest counts of 10-yr flood peaks, followed by Florence (2018). The top 10 storms account for 32% of annual flood peaks, 58% of 10-yr flood peaks, and 75% of record floods produced by all TCs, highlighting the critical role of a small portion of storms in TC flooding. Results also shed light on the mixture distribution of flooding in the Carolinas: the prominent role of TCs in the upper tail of flood peak distribution (e.g., Smith et al. 2010; Villarini and Smith 2010) is principally dominated by a handful of storms (see also Smith et al. 2018). Annual flood peak is a potential candidate for ranking storms. This metric, however, is less useful in reflecting the flood magnitude.

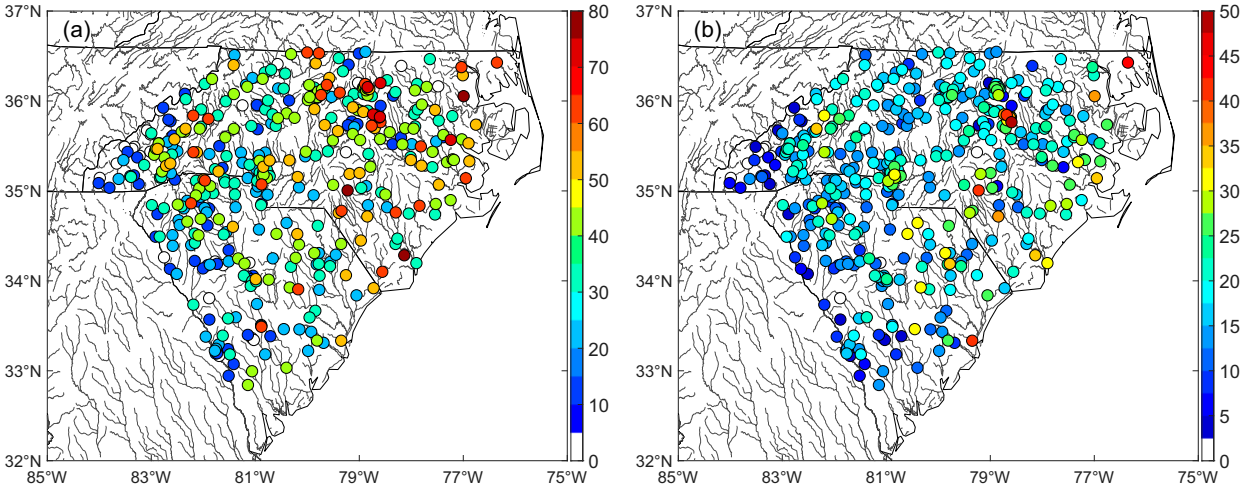

FIG. 4. Percentage (%) of (a) top 10 flood peaks and (b) annual flood peaks that were produced by tropical cyclones.

TABLE 2. A list of top 10 tropical cyclones in terms of counts of 10-yr flood peaks in the Carolinas. ET is extratropical transition.

No.	Name	Year	Month	Flood ratio ≥ 1	Annual flood peak (No.)	Record flood (No.)	Landfall intensity (m s^{-1})	Ave. inland intensity (m s^{-1})	ET status
1	1940 South Carolina	1940	8	61	91	33	39	26	Non-ET
2	Florence	2018	9	57	88	23	54	30	Non-ET
3	1945 Homestead	1945	9	54	104	23	36	26	Non-ET
4	Matthew	2016	10	54	75	13	57	41	ET
5	Fran	1996	9	41	66	17	54	34	Non-ET
6	Jerry	1995	8	38	70	16	18	13	Non-ET
7	Floyd	1999	9	36	66	19	57	43	ET
8	Hilda	1964	10	32	43	7	18	18	ET
9	Frances	2004	9	29	110	7	31	19	Non-ET
10	Marco	1990	10	29	61	11	21	11	ET

We examined storm properties of the top 10 TCs (Table 2). The occurrence year of the 10 storms covers a relatively wide range from 1940 to 2018. There are more than two storms in three decades, the 1940s, 1990s, and 2010s. This clustering, however, is not in accordance with annual counts of landfalling TCs in the Carolinas (Fig. 2a). The occurrence month of the 10 TCs concentrates in peak hurricane season, ranging from August to October. There are striking contrasts in the storm intensity of the 10 TCs: four storms reached major hurricane intensity (≥50 m s^{-1}) at landfall while three storms reached slightly above tropical storm intensity (≥18 m s^{-1}) at landfall (Table 2). Statistical analyses based on satellite rainfall products (e.g., Jiang et al. 2008a; Lonfat et al. 2004) and future projections based on climate model simulations (e.g., Liu et al. 2019) both identified storm intensity as an important driving force for TC rainfall rate. The relatively weak storms, however, demonstrate that high intensity is not a necessary condition for producing extreme rainfall and flooding. Hurricane Hilda (1964) produced heavy rainfall hundreds of kilometers ahead of its track in the Carolinas, principally resulting from interactions with frontal boundaries in the east coast. For Tropical Storm Marco (1990), the torrential rainfall distant from the storm center was principally linked to coastal frontogenesis ahead of the storm [see Srock and Bosart (2009) for details]. The interaction with a costal front was also a key element of heavy rainfall associated with Matthew (Powell and Bell 2018). Given the frontal nature of rainfall and baroclinic features in storm structures, we broadly regard these storms as extratropically transitioning TCs (Evans and Hart 2003; Jones et al. 2003). Hurricane Floyd (1999), which produced 36 10-yr flood events in the Carolinas (Table 2), was also a transitioning storm although the interaction with an upper-level trough played a more prominent role in the transitioning process (Atallah and Bosart 2003; Colle 2003). In addition to these storms, the 1945 Homestead Hurricane, Hurricane Fran (1996), and Frances (2004) completed extratropical transition after passing over the Carolinas, extending their impacts to the mid-Atlantic region and New England.

There is large diversity in the spatial distribution of flood peaks produced by the top 10 TCs (see the top four in Fig. 5 for example). The left-of-center distribution of flood peaks is seen in Hurricane Matthew (2016), reflecting rainfall distribution of such type of events shaped by frontal boundaries (Powell and Bell 2018). In contrast, the 1940 South Carolina Hurricane and Hurricane Florence exhibited right-of-center distribution of flood peaks while there was no strong preference for left- or right-of-center distribution of flood peaks for the 1945 Homestead Storm. Rainfall distributions of the three storms are dominated by spiral rainbands characteristic of mature TCs (e.g., Houze 2010; Yang et al. 2019a). Their contrast in spatial distribution of flood peaks is linked to diversity in track properties. East-to-west movement is a key element of storm track of 1940 South Carolina and Florence while 1945 Homestead principally exhibited a south-to-north movement during the passage over the Carolinas.

Clustering of record floods and 10-yr flood peaks produced by 1940 South Carolina, Frances in 2004 (Lonfat et al. 2007), and Hilda is seen in the eastern margin of Blue Ridge Mountains (west North Carolina; see Fig. 1), reflecting the central role of orographic rainfall mechanism in amplifying flood peak extremes in North Carolina. Fran is another prominent example of orographic enhancement of storm rainfall and resultant flooding in the central Appalachians region, but in Virginia (Sturdevant-Rees et al. 2001).

c. *The Great Flood of 1916*

The Great Flood of 1916 is not covered in analyses above and is probably the most damaging flooding that hit western North Carolina, with the most severe flooding occurring on French Broad River watershed. The primary drivers of the devastating flooding were two consecutive landfalling hurricanes (see Fig. 6 for tracks of the two events). The first hurricane (1916 Gulf Coast hurricane) initiated as a tropical depression in the southwestern Caribbean Sea on 28 June and intensified to a category 3 hurricane (54 m s^{-1}) prior to making landfall near Gulfport, Mississippi, on 5 July. The storm weakened to tropical storm intensity on 6 July and meandered across Mississippi, Alabama, and Tennessee for several days as the northward movement was suppressed by high pressure systems to the north of the track. Similar to Hurricane Harvey in 2017 (e.g., Yang et al. 2019a), the slow storm motion is an important element of heavy rainfall produced along the storm track. The second hurricane (the 1916 Charleston Hurricane) originated on 11 July north of the Bahamas, reached major

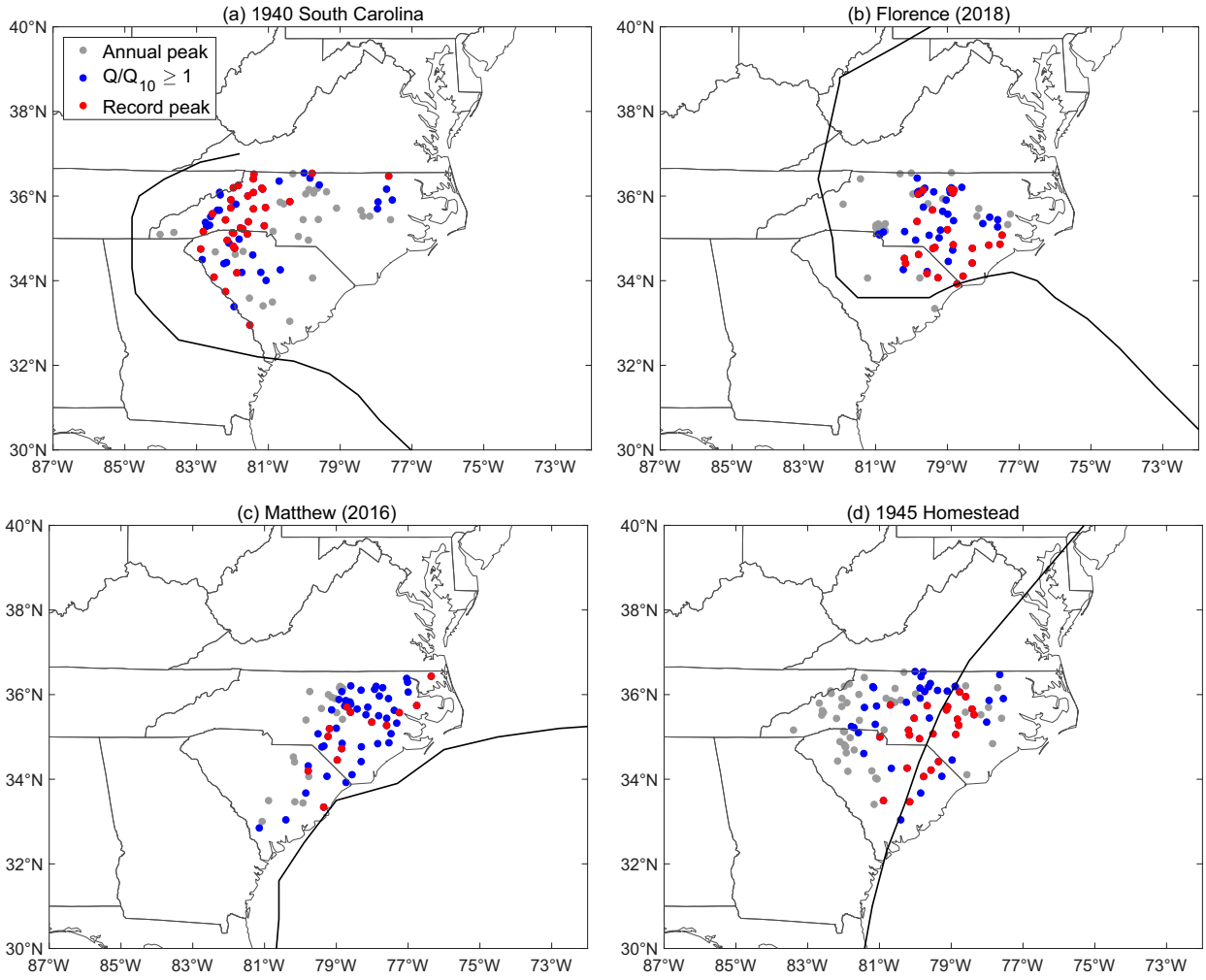

FIG. 5. Maps showing annual flood peaks (gray circle), flood peaks with flood ratio larger than 1 (blue circle), and record floods (red circle) from the top four tropical cyclones selected based on counts of 10-yr flood peaks. Storm tracks are shown in black lines.

hurricane intensity (51 m s^{-1}) on 13 July, and made landfall near Charleston, South Carolina, as a category 2 hurricane on 14 July.

From 8 to 11 July 1916, the first hurricane produced rainfall of approximately 75–150 mm over the French Broad River watershed, which led to an increase of gauge height to 2.7 m (8.8 feet), 1.5 m higher than the flood stage. Although the water level dropped by more than 1 m on July 15, the saturated soil conditions set the stage for the coming devastating flooding. The second hurricane weakened to a weak low near the Smoky Mountains on 15 July but produced rainfall of more than 250 mm over French Broad River watershed for the next 24 h. An unofficial rain gauge at Altapass on the eastern slope of the Smoky Mountains recorded a 24-h rainfall total of 564 mm (22.2 in.) on 16 July, setting the state record of North Carolina.

The most extreme 1916 flooding occurred on the French Broad River at Asheville (drainage area of 2448 km^2; USGS ID 03451500), which crested at a gauge height of 5.9 m (23.1 ft) with a peak discharge of 3115 m^3 s^{-1}. Annual flood peak and gauge height time series at Asheville highlight the extreme magnitudes of the Great Flood of 1916 (Fig. 7). The 1916 peak at Asheville is 2.6 times larger than the second-largest peak produced by Hurricane Ivan (2004) based on the available record of 124 years. Using the entire record at Asheville, the estimated 100-yr flood peak is 1508 m^3 s^{-1} based on the generalized extreme value (GEV) distribution, approximately half of the 1916 flood peak. The estimated return interval for the 1916 peak at Asheville is approximately 2000 years. If the 3115 m^3 s^{-1} peak is excluded, the 100-yr flood peak decreases to 1213 m^3 s^{-1} and the return period of the 1916 flood peak increases to approximately 50 000 years. The Great Flood of 1916 destroyed numerous homes and roads, three main bridges, and almost all dams for hydropower upstream of Asheville, causing approximately 80 deaths and estimated economic losses of $21 million (1916 U.S. dollars).

The impact of the two successive storms is a key element of the devastating flooding in the western North Carolina. A similarly prominent example is Hurricanes Connie and Diane

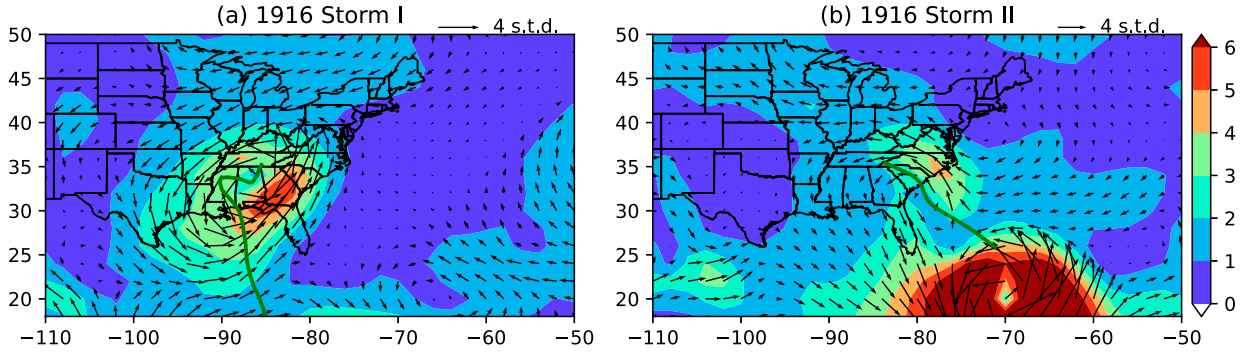

FIG. 6. The ratio (shaded) of vertically integrated water vapor flux anomaly to the standard deviation computed based on the period of 1910–2014. Note that the water vapor flux anomaly and standard deviation are computed based on the same storm period as the two 1916 storms over 1910–2014. Arrows indicate the direction and magnitude of the ratio. The green line indicates storm track.

in 1955 that produced extreme flooding in New England. This highlights the role of multievent compounding in driving extremes.

Orographic enhancement played an important role in the extreme rainfall for the Great Flood of 1916. Water vapor flux is a key ingredient of precipitation. Anomalies of vertically integrated water vapor flux for the two storms are 2–6 times greater than the standard deviation for the same storm period over 1910–2014, reflecting the extreme nature of storm rainfall (Fig. 6). The spatial pattern of the water vapor flux anomaly highlights the moisture supply from the Gulf of the Mexico for the first storm and from the mid-Atlantic for the second storm. Note that the water vapor flux anomaly is computed based on the mean flux over the same date as the 1916 storms over 1910–2014.

4. Hurricanes Matthew (2016) and Florence (2018)

In this section, we examine extreme rainfall from Matthew and Florence and highlight the contrasting nature of the two storms. We also characterized hydroclimatology and hydrology of extreme flooding for the two storms. Locations of river basins are shown in Fig. 8.

a. Rainfall

We computed storm total rainfall accumulations from hourly rainfall fields from Stage IV. We examined the spatial and temporal evolution of rainfall fields using the radius–time diagram (see also Liu and Smith 2016; Villarini et al. 2011). Analyses are presented in four quadrants: front-left (left and ahead of the track), front-right, back-left, and back-right.

For Matthew, rainfall accumulations exceeding 200 mm covered a broad area, extending from southwest to northeast through the eastern Carolinas (Fig. 9). Maximum rainfall that exceeded 400 mm was concentrated in downstream portions of Little Pee Dee River and Cape Fear River. A major rainfall episode concentrated on 8 October 2016 (see Fig. 10 for temporal variation of rainfall fields) was principally responsible for flood peaks in these regions. A prominent feature of rainfall accumulations from Matthew is the striking land–sea contrast with a sharp spatial gradient of rainfall along the coastal lines, which may be partially attributed to the land–sea contrast in surface roughness (Li et al. 2015; Yang et al. 2019a; Zhang et al. 2018). The pronounced left-of-center rainfall distribution (Fig. 9), dominated by heavy rainfall in the front-left quadrant over extensive range from the storm center (Fig. 10), was associated with extratropical transition of the storm (Atallah et al. 2007; Atallah and Bosart 2003; Colle 2003; Jones et al. 2003; Liu et al. 2018; Liu and Smith 2016). The radius of heavy rainfall exceeding 10 mm h^{-1} in the front-left quadrant exhibited large temporal variability, reflecting temporal evolution of storm structure and organization of frontal rainbands. Heavy rainfall in inner-core regions

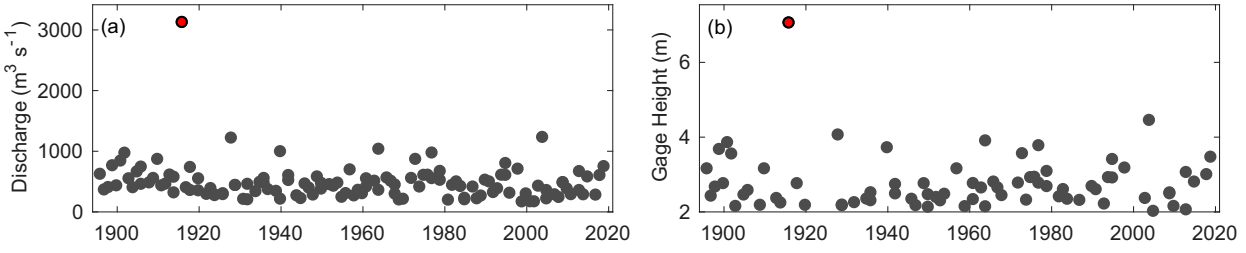

FIG. 7. (a) Annual flood peak and (b) gauge height time series for French Broad River at Asheville. Red circles indicated flooding produced by the Great Flood of 1916.

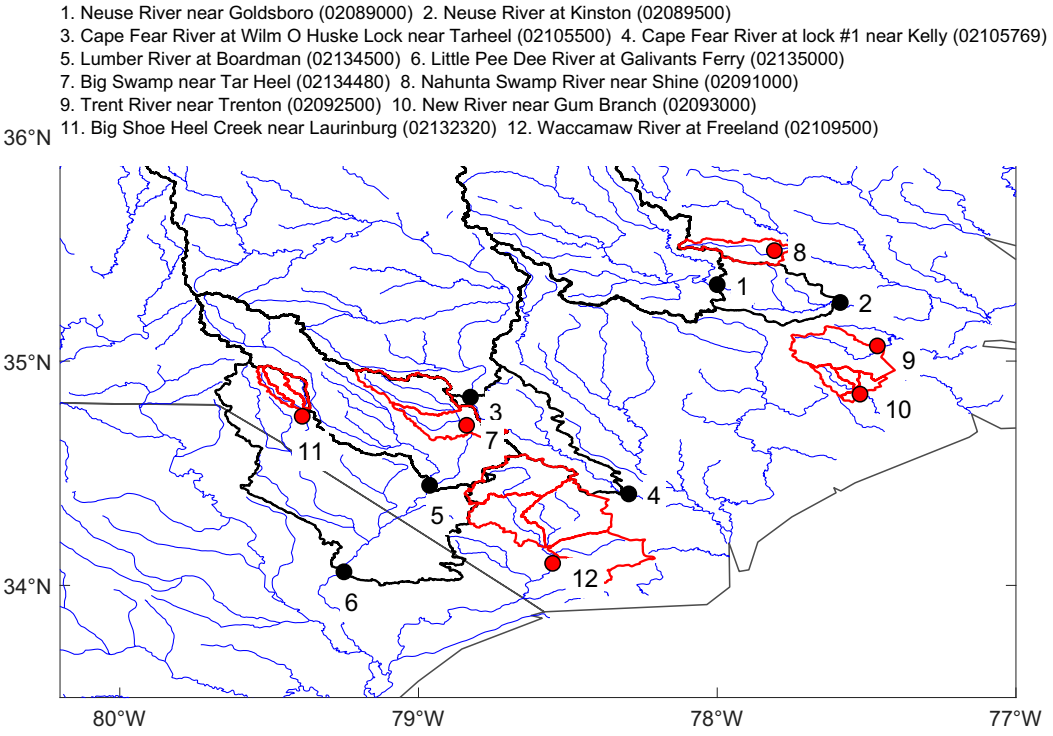

FIG. 8. Study area for flood events produced by Hurricane Matthew and/or Florence. Stream gauging stations and basin boundaries are shown in black for six relatively large river basins and in red for watersheds with flood ratios larger than 5. Numbers in the parentheses are USGS ID numbers. See Figs. 16 and 17 and Table 3 for details on flood analyses.

in the front quadrants disappeared after landfall, suggesting the decaying of inner rainbands. The interaction of the storm and frontal boundary played a critical role in the temporal variation of outer rainbands.

Extreme storm total rainfall for Florence was concentrated over a smaller region than Matthew but with much greater maximum accumulations (Fig. 11). Maximum rainfall up to 1000 mm was concentrated in Trent River, New River, and Big Shoe Heel Creek in the coastal areas. Heavy rainfall for Florence extended from southeast to northwest through the eastern Carolinas, in contrast to the southeast-to-northwest orientation of rainfall for Matthew. The rainfall distribution of Florence was dominated by rainbands in inner-core regions before 0000 UTC 15 September (Fig. 12). In contrast, spirally outer rainbands particularly in the back-right quadrant played a more prominent role in the major rainfall episode during the 15–16 September period, suggesting changes toward a more loosely organized storm structure.

Although Matthew and Florence produced heavy rainfall over similar regions, there are substantial differences in the properties of the two storms. Matthew moved along coastal lines while Florence moved farther inland. The left-to-center rainfall distribution for Matthew was dictated by frontal rainbands associated with extratropical transition of the storm. In contrast, rainfall for Florence exhibited a right-of-center concentration, principally resulting from spiral outer rainbands that resembled features of distance rainbands of typical TCs that are less constrained by the storm inner-core vortex than eyewall bands [see Houze (2010) for more details of distant rainbands]. Another important distinction between the two storms is the duration of the extreme rainfall episode resulting from translational speed differences. Heavy rainfall for Matthew in the Carolinas was concentrated on a one-day period (8 October 2016) due to relatively high storm speed, a typical feature of storms undergoing extratropical transition. In contrast, the rainfall episode of Florence was over a 3-day period (14–16 September 2018) due to a low translation speed, which is a key element of extreme rainfall production, similar to Harvey in 2017 (Yang et al. 2019a).

Despite the contrast of the two hurricanes in many storm properties, a common feature of the two is large moisture transport. For both hurricanes, the ratio of storm-related vertically integrated water vapor flux to the sample 10-yr flux exhibited large values in the mid-Atlantic areas (Figs. 13 and 14). The spatial map of the ratio for Matthew also highlighted the moisture sources from the tropical Atlantic near Florida (Fig. 13). The 850-hPa moisture convergence, defined as the convergence of the product of specific humidity and wind speed, is a good indicator of the large-scale atmospheric ascent. Locations of strong moisture convergence (Figs. 13 and 14) roughly correspond with heavy rainfall (Figs. 9 and 11), suggesting the role of low-level convergence in producing rainfall. In addition to moisture flux,

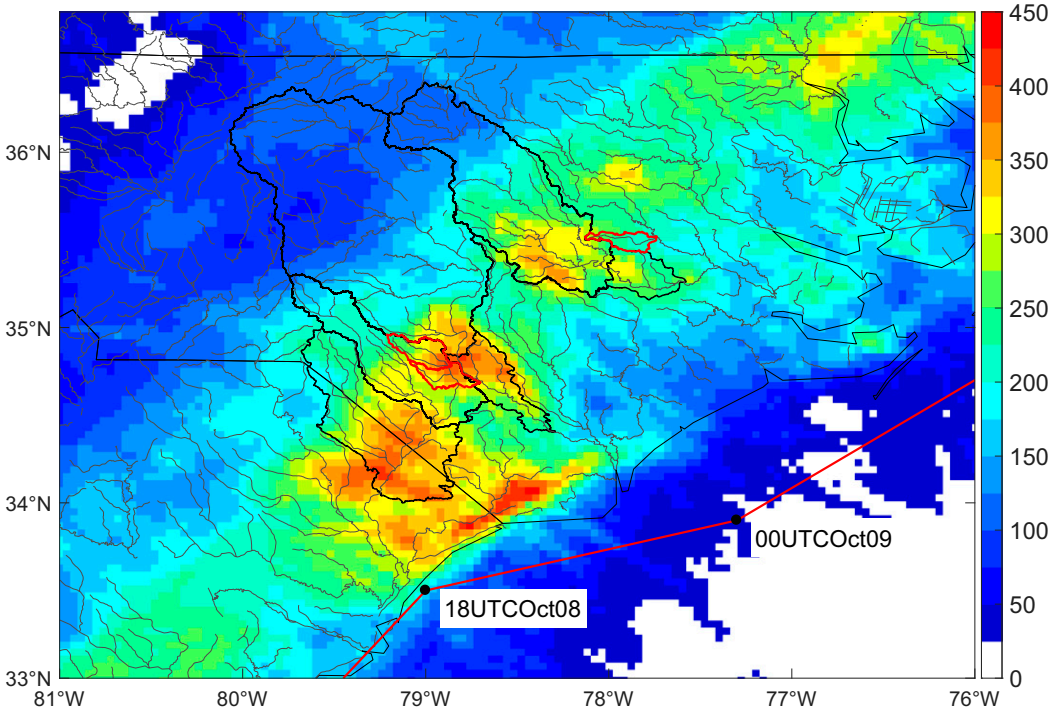

FIG. 9. Stage IV–based storm total rainfall (mm) produced by Hurricane Matthew (2016). The red line indicates the storm track of Matthew. Similar to Fig. 8, the basin boundaries for relatively large river basins and watersheds with flood ratio larger than 5 are shown in black and red, respectively.

we examined PW for Florence from measurements by two GPS sites and simulations by WRF model (Fig. 15). For the North Carolina Castle Hayne (NCCH; 2007) site, the PW value increased from approximately 50 mm at 1200 UTC 13 September to the maximum of 82.7 mm at 1145 UTC 14 September (Fig. 15a). WRF exhibited good skill in simulating the trend and magnitude of PW. Both WRF simulation and GPS measurement highlighted high values of PW during the storm period. The South Carolina Longs (SCHY) site showed similar results to NCCH with PW maximum at 84.1 mm (Fig. 15b). For reference, the second-largest PW value is 71.4 mm (produced by Hurricane Dorian in 2019) for NCCH and 74.7 mm for SCHY over the period of 2009–19.

b. *Flooding*

We used time series of annual flood peaks to examine the hydroclimatology of flooding for the two hurricanes in six relatively large river basins (see Fig. 8 for locations of river basins) over eastern North Carolina (Fig. 16). Matthew produced record flood peaks in the Neuse River near Goldsboro (Fig. 16a; 1512 $m^3 s^{-1}$ at 6211 km^2) and at Kinston (Fig. 16b; 1082 $m^3 s^{-1}$ at 6969 km^2) in North Carolina from a record of 88 years. For both Matthew and Florence, the flooding in the Neuse River was produced by rainfall concentrated in the southern (downstream) portion of the basin (see Figs. 9 and 11 for storm total rainfall from Stage IV). The second-largest flood peak in the Neuse River basin was produced by Hurricane Floyd in 1999 and the third-largest peak by Florence (Figs. 16a,b). For Cape Fear River at the William O. Huske Lock (drainage area of 12 561 km^2) and at Lock #1 near Kelly (drainage area of 13 605 km^2) in North Carolina, Florence set the new record of flood peak that was previously produced by Matthew (Figs. 16c,d). Increase of storm total rainfall from northwest to southeast is seen in the Cape Fear River basin for the two storms, similar to in the Neuse River basin (Figs. 9 and 11). The replacement of Florence over Matthew for record flood is also seen in the Little Pee Dee River at Galivants Ferry (Fig. 16f; drainage area of 7223 km^2). In contrast, Matthew retained the record flood in the Lumber River at Boardman (drainage area of 3179 km^2) with the second-largest peak by Florence (Fig. 16e). The "competition" of Matthew and Florence for the record of flooding reflects the critical role of the complex distribution of rainfall fields in flooding.

The most striking feature of the flooding from these two storms was the discharge peak in the Trent River near Trenton in North Carolina (1917 $m^3 s^{-1}$ at 435 km^2), which was 12.6 times greater than the sample 10-yr flood peak. The 1917 $m^3 s^{-1}$ peak produced by Florence is approximately triple the second-largest flood peak due to Floyd in 1999 from a record of 67 years (Fig. 17a). Based on the GEV distribution, the estimated return interval for the Florence peak near Trenton is approximately 700 years, which increased to approximately 2800 years if the peak was omitted. The record flooding in the Trend River basin resulted from rainfall episodes on 14–16 September (Fig. 17b) due to enhanced rainbands (Fig. 11). Hourly rainfall accumulations in the basin ranged from 5 to

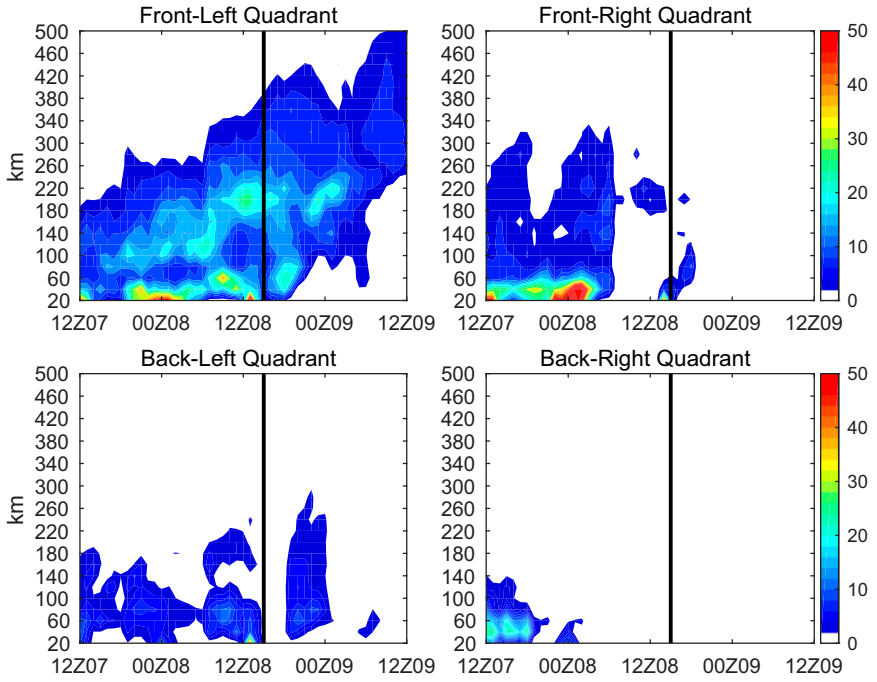

FIG. 10. The radius–time diagram of storm rainfall rate (mm h^{-1}) for Hurricane Matthew (2016) based on Stage IV rainfall fields at hourly interval. The four quadrants are defined with respect to the storm motion of Matthew. The black line indicates the time of landfall.

20 mm for the first 24 h and burst to 30 mm for the next 7 h before rapidly dropping to below 5 mm, reflecting complex storm structure and evolution (Fig. 17b). Storm total rainfall in Trent River ranged from 700 mm in the eastern portion of the basin to 550 mm in the western portion of the basin, with a mean accumulation of 636 mm (Fig. 11). Estimated runoff in the basin is 1049 mm based on discharge time series (Fig. 17c), much greater than the rainfall

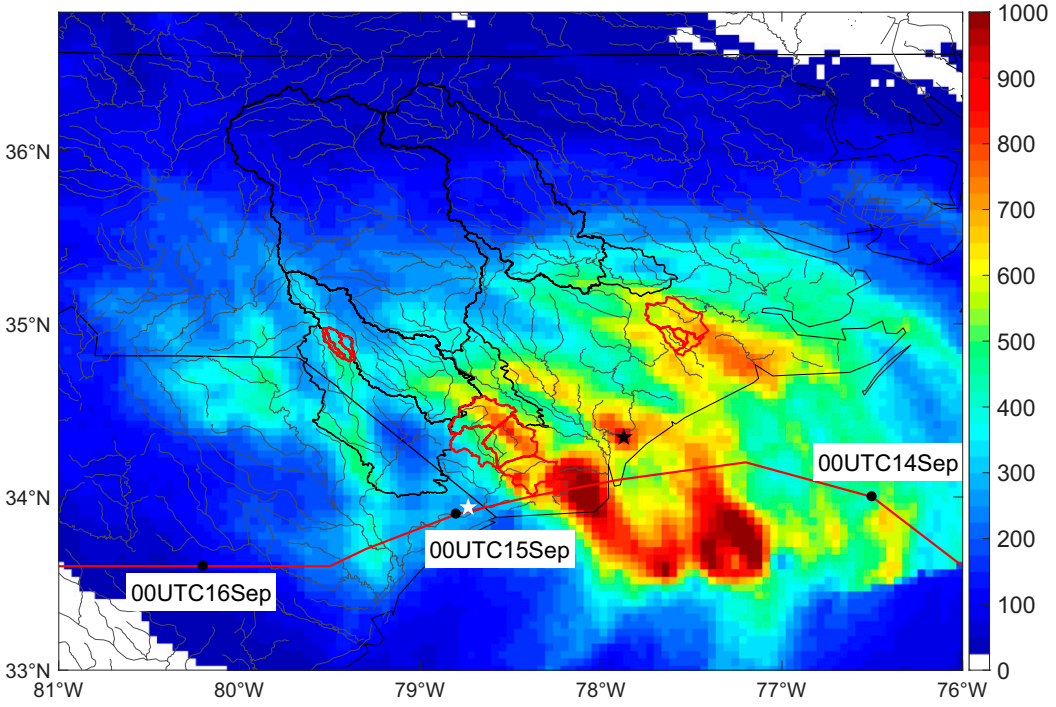

FIG. 11. As in Fig. 9, but for Hurricane Florence (2018). The black (white) star shows the location of the NCCH (SCHY) site.

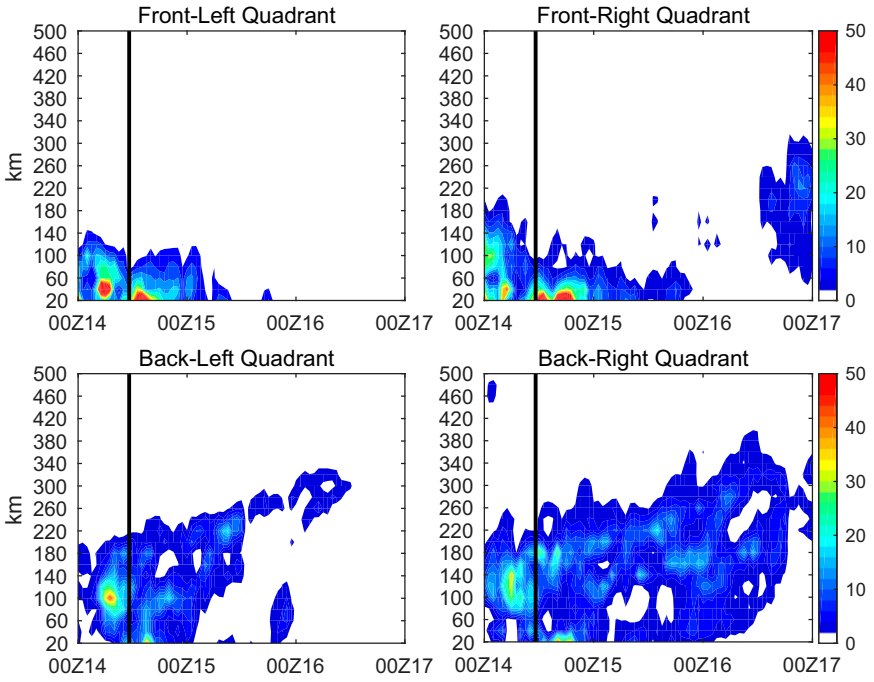

FIG. 12. As in Fig. 10, but for Hurricane Florence (2018).

accumulation and even the rainfall maxima. The temporal resolution of the discharge data sharply increased from 15 min to 6-hourly right before the storm visit, which is very likely a primary cause for the overestimation of runoff. In addition, a rain gauge from the Community Collaborative Rain, Hail and Snow Network (CoCoRaHS; Cifelli et al. 2005) reported a storm total rainfall of 465 mm within the basin, in comparison to 554 mm from Stage IV at the same location.

Additional perspective on the extreme flooding produced by these two storms is provided by examining flood ratios (Smith et al. 2018; Yang et al. 2019b). Matthew produced two flood events with flood ratio greater than 5 while Florence

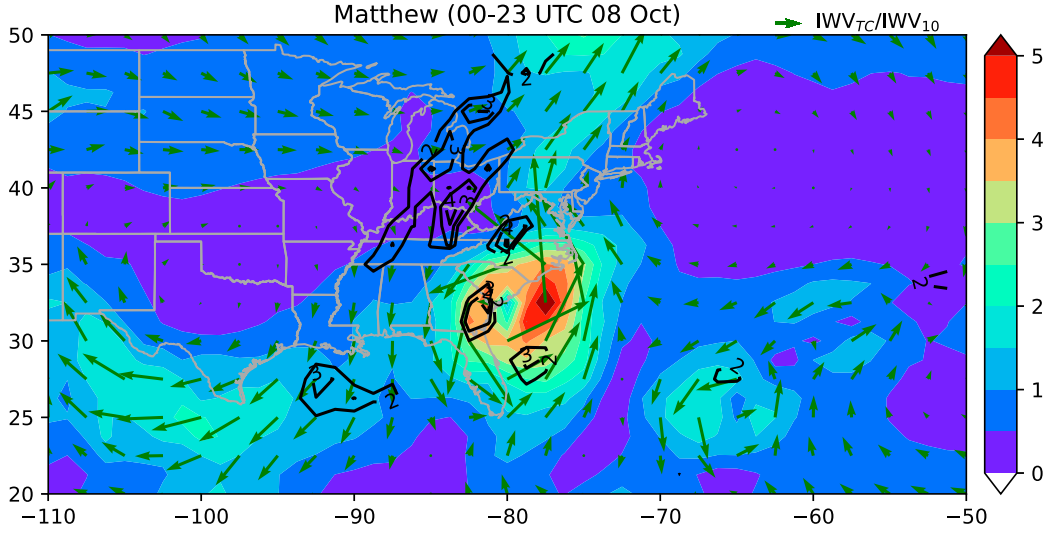

FIG. 13. The ratio (shaded) of vertically integrated water vapor flux for Matthew to sample 10-yr flux over the same date (8 Oct 2016) as Matthew estimated over the based period of 1958–2018. Arrows indicate the direction and magnitude of the ratio. The black contour indicates the ratio of 850-hPa moisture convergence (i.e., the convergence of the product of specific humidity and wind speed) for Matthew to sample 10-yr moisture convergence estimated over the period of 1958–2010.

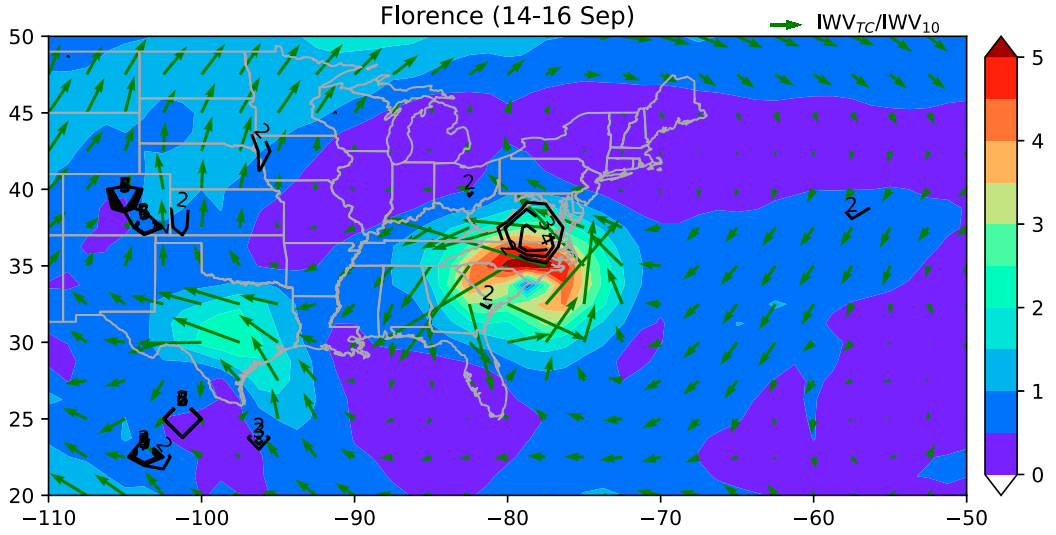

FIG. 14. As in Fig. 13, but for Florence, focusing on the storm period of 14–16 Sep 2018.

produced four such events, including the flood peak in the Trend River near Trenton (see Table 3 for details and Fig. 8 for locations of river basins). For Matthew, the flood ratio was 5.8 in the Big Swamp near Tar Heel and 5.3 in the Nahunta Swamp River near Shine (Table 3). Rainfall in Big Swamp near Tar Heel ranged from up to 400 mm in the eastern portion of the basin to 200 mm in the western portion of the basin (Fig. 9). Mean rainfall in the basin was 327 mm, runoff was 199 mm, and the runoff ratio was 61% (Table 3). The runoff ratio in the Nahunta Swamp River near Shine was 85%, estimated from rainfall accumulations of 237 mm and runoff of 202 mm. The strikingly large runoff ratio is probably due to underestimation of rainfall by Stage IV. A handful of rain gauges from CoCoRaHS, located near the Nahunta Swamp river basin, reported rainfall accumulations of 270–390 mm, higher than the basinwide mean rainfall (237 mm).

Florence produced a mean rainfall accumulation of 650 mm in the New River near Gum Branch (drainage area of

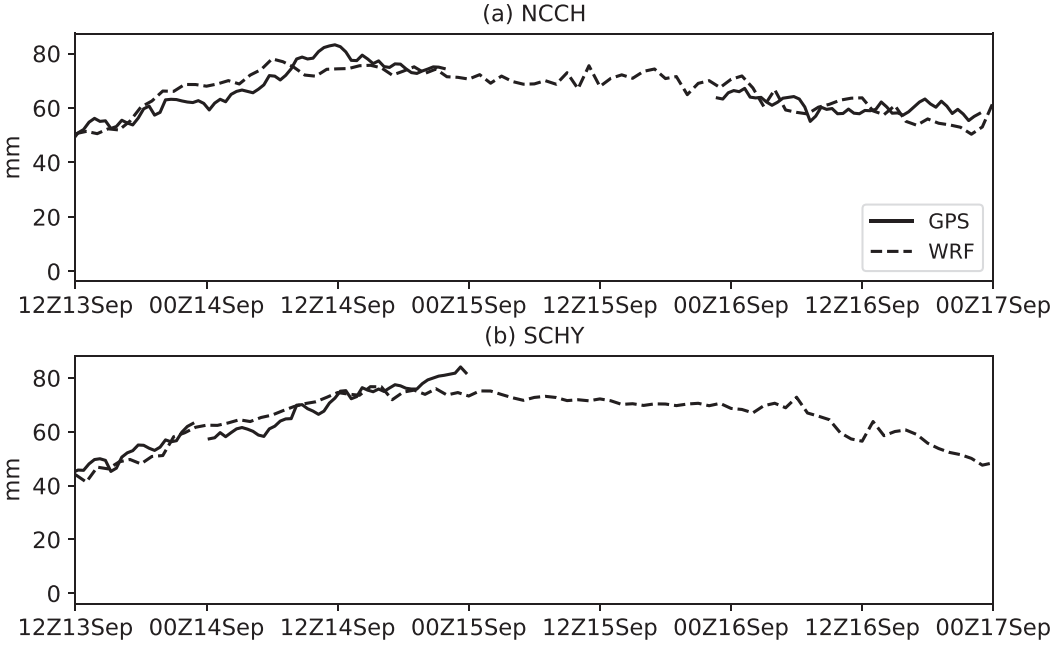

FIG. 15. Time series of column-integrated PW (mm) over the storm period of Florence from GPS measurements at (a) NCCH and (b) SCHY. See Figs. 1 and 11 for locations of the two sites. PW from WRF simulations over the same sites are also shown.

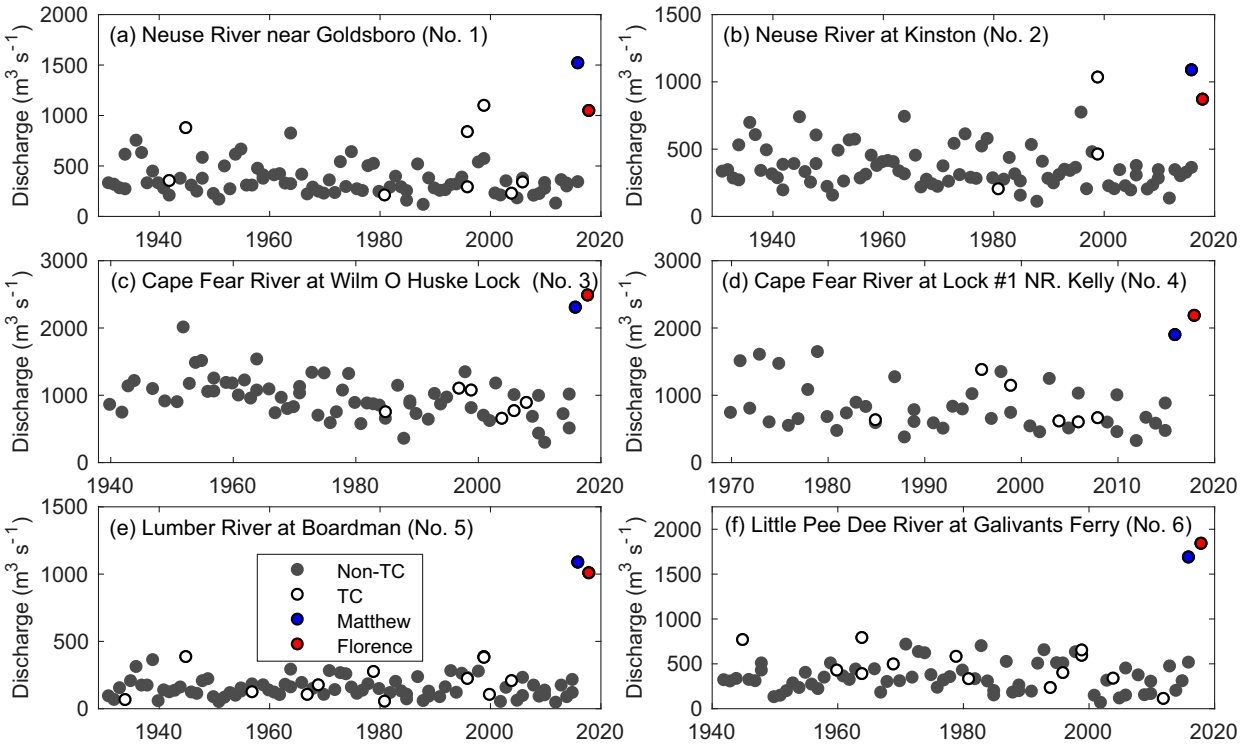

FIG. 16. Annual flood peak time series for six relatively large river basins. White circles indicate flood peaks associated with tropical cyclones (TCs) while gray circles other flood-generating systems. Blue circles indicate flood peaks produced by Hurricane Matthew (2016) while red circles indicate those by Hurricane Florence (2018). See Fig. 8 for locations of river basins.

243 km^2), resulting in a flood peak of 991 m^3 s^{-1}, 6.9 times greater than the 10-yr peak. Estimated runoff was 574 mm, and the runoff ratio was 88%. Similar to the Trent River near Trenton, the interval of discharge in the New River was 4-hourly, probably leading to uncertainty to runoff estimation. Storm total rainfall in Waccamaw River at Freeland ranged from 800 mm in the eastern portion of the basin to 400 mm in the western portion of the basin. The mean value of rainfall accumulation was 620 mm and estimated runoff is 374 mm, resulting in a runoff ratio of 60%. For Big Shoe Heel Creek near Laurinburg, Florence produced a much less rainfall accumulation (385 mm) in this farther inland basin. With estimated runoff of 172 mm, the runoff ratio is 45%.

5. Summary and conclusions

We have examined TC-induced flooding in the Carolinas during the period 1930–2018 through analyses of annual flood peak observations from 411 USGS stream gauging stations. The hydroclimatology, hydrometeorology, and hydrology of extreme flooding from two recent hurricanes (Matthew in 2016 and Florence in 2018) are examined through analyses of flood peaks and analyses of the temporal and spatial distribution of extreme rainfall. The major findings of this study are summarized as follows.

1) TCs are key flood agents in the Carolinas. They account for 16% of the annual flood peaks at USGS stream gauging stations during the period 1930–2018. This percentage increases to 28% for top 10 annual flood peaks, 55% (227/411) for record flood peaks, and 91% (20/22) for flood peaks with a flood ratio larger than 5. TCs play an increasingly prominent role for extreme flood events, reflecting the nature of mixture distributions of flooding in the Carolinas. Based on the spatial flood maps, the flood peaks associated with TCs in inland regions are comparable to coastal areas. A cluster of flood peaks located along the eastern margin of the Appalachians (western regions of North Carolina) highlight the role of orographic precipitation mechanisms for tropical cyclone–induced flood peaks.

2) TCs produce, on average, more than one annual peak per year and record flood peaks every two to three years. Another important feature of tropical cyclone–related flooding is the dominant role of a small number of storms. The top 10 storms account for nearly 1/3 of the annual flood peaks and more than 2/3 of record flood peaks. Analyses of the 10 storms highlight common elements and diversity of storm properties that are responsible for the flood peaks. The 10 storms are concentrated during the period from August to October, the key hurricane season. Diversity of track properties through the Carolinas is found for the 10 storms. High storm intensity is not a necessary condition for producing flood peaks; 4 of the 10 storms made landfall close to tropical storm intensity. The locations of flood peaks relative to storm tracks show large contrasts among storms, reflecting the distinctive nature

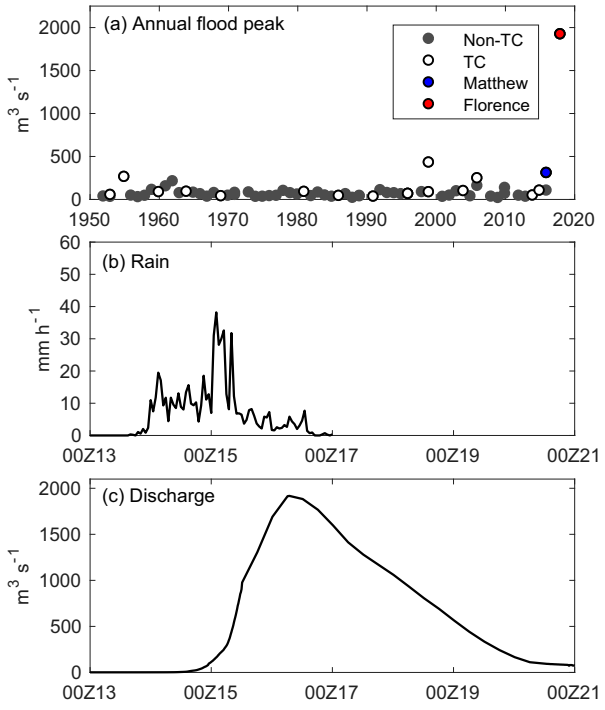

FIG. 17. (a) Annual flood peak time series for Trent River near Trenton (drainage area of 435 km^2). See Fig. 8 for the location of the basin. (b) Time series of basin-averaged rainfall at hourly interval based on Stage IV rainfall fields during the passage of Florence and (c) time series of discharge.

of spatial patterns of storm rainfall. Extratropical transition is an important element of extreme rainfall and flooding with 4 of the 10 storms undergoing extratropical transition in the Carolinas.

3) The Great Flood of 1916 was among the most devastating floods in western North Carolina. The most striking feature of this flooding is the flood peak of 3115 m^3 s^{-1} in French Broad River at Asheville, which is 2.6 times greater than the second-largest peak from a record of 124 years. The estimated return interval for the flood peak at Asheville based on the GEV distribution is 2000 years, which would increase to approximately 50 000 years if the 3115 m^3 s^{-1} peak was omitted. The primary cause of the Great Flood of 1916 is two "back-to-back" hurricanes in the North Carolina. Saturated soil conditions due to the first storm set the stage for the coming devastating flooding produced by the second hurricanes. Furthermore, orographic enhancement is a key element of extreme rainfall in the Blue Ridge Mountain/Smoky Mountain regions.

4) Hurricanes Matthew (2016) and Florence (2018) were examined to assess extreme rainfall and resultant flooding. The two hurricanes produced flooding over similar river basins but show contrasting storm properties, highlighting the diverse nature of TCs that produce extreme flooding. Matthew (2016) moved along the coast and produced peak rainfall in its left quadrant (on shore), the region accounting for record flood peaks at 13 stations and two flood peaks with flood ratio larger than 5. In contrast, Florence (2018) moved inland from the Atlantic. Extreme rainfall from Florence was concentrated in the right quadrant of the storm and accounts for record flood peaks in 23 stations and five flood peaks with an upper tail ratio larger than 5; for many stations Florence replaced Matthew as the flood of record. The Trent River near Trenton (drainage area of 435 km^2) experienced a record flood peak from Florence of 1917 m^3 s^{-1}, a value that is 12.6 times larger than the 10-yr flood magnitude from a record of 67 years.

5) Extreme rainfall in the Carolinas from Matthew was dominated by the rain episode on 8 October 2016, which was organized through a fast-moving elongated frontal rainband; extratropical transition played a major role in structure and organization of extreme rainfall. The heterogeneity of the frontal bands dictated the temporal and spatial distribution of rainfall that determined the spatial variation of flooding. Another prominent feature of rainfall from Matthew is the sharp spatial gradient of rainfall along the coast, which may be partially attributed to the land–sea contrast in surface roughness. In contrast to Matthew, Florence exhibited typical hurricane structure with extreme rainfall principally associated with outer spiral rainbands. Florence moved more slowly than Matthew due to

TABLE 3. Flood summary for selected river basins produced by Hurricane Matthew and/or Florence.

No.	Station name	USGS ID	Record length	Area (km^2)	Hurricane	Peak (m^3 s^{-1})	Date	Q/Q_{10}	Runoff (mm)	Rain (mm)
7	Big Swamp near Tar Heel	02134480	33	593	Matthew	549	9 Oct 2016	5.8	199	327
8	Nahunta Swamp River near Shine	02091000	64	208	Matthew	385	9 Oct 2016	5.3	202	237
9	Trent River near Trenton	02092500	67	435	Florence	1917	16 Sep 2018	12.6	—	636
10	New River near Gum Branch	02093000	55	243	Florence	991	15 Sep 2018	6.9	—	650
11	Big Shoe Heel Creek near Laurinburg	02132320	31	216	Florence	173	17 Sep 2018	6.0	172	385
12	Waccamaw River at Freeland	02109500	77	1760	Florence	1518	19 Sep 2018	5.7	374	620

the impact of a blocking high in the northwest, another important element of extreme rainfall production. The major rain episode of Florence in the Carolinas extended for three days, 14–16 September. Two GPS sites measured strikingly high PW with maxima of 82.7 and 84.1 mm, respectively. The climatological analyses of the vertically integrated water vapor transport from the two storms highlight the critical role of anomalous moisture flow from Atlantic Ocean in producing extreme rainfall and resultant flooding.

This study highlights the diverse nature of storm properties for TCs that produce extreme rainfall and flooding in the Carolinas, which brings challenges to projections of future TC flood hazard under the context of climate warming. In addition to storm dynamics, complex hydrological response processes also add difficulties to the future projection. Future work can take advantage of the high-resolution dynamical models from the Coupled Model Intercomparison Project (e.g., Roberts et al. 2020) and synthetic TC models (e.g., Bloemendaal et al. 2020) to project future TC flood risk in the Carolinas.

Possible regime shift of TC flooding highlights the need for improved flood control infrastructure, often designed based on estimates of probable maximization precipitation (PMP). The reliability of PMP depends on the quality of historical meteorological data. Caldwell et al. (2011) found that Hurricane Fran and Floyd exceed PMP from Hydrometeorological Report 51 (HMR 51) conducted by NOAA in terms of a few aspects of extreme rainfall, highlighting the need for updating PMP estimates. Matthew and Florence examined in this study are important candidates for updating PMP analyses due to flood severity, which can provide new guide for assessing and designing flood-control infrastructures in the Carolinas.

Acknowledgments. This work was supported by the National Science Foundation (Grants EAR1520683 and AGS-1262099), Award NA14OAR4830101 from the National Oceanic and Atmospheric Administration (NOAA), U.S. Department of Commerce, and Award 80NSSC19K0482 from the National Aeronautics and Space Administration. This work is also supported in part by the School of Engineering and Applied Sciences and the Carbon Mitigation Initiative at Princeton University.

Data availability statement. The discharge data are obtained from U.S. Geological Survey (available online at https://waterdata.usgs.gov/nwis/sw). The best track data from the Atlantic hurricane database are obtained from National Hurricane Center (available online at https://www.nhc.noaa.gov/data/#hurdat). Stage IV rainfall data are obtained from NOAA National Centers for Environmental Prediction (NCEP) (available online at https://data.eol.ucar.edu/cgi-bin/codiac/fgr_form/id=21.093). Precipitable water vapor data are obtained from SuomiNet Global Positioning System network (available online at https://www.unidata.ucar.edu/data/suominet/). The 20th Century Reanalysis data, Japanese 55-year Reanalysis data, and the NCEP FNL (Final) Operational Global Analysis data are provided by the NOAA/OAR/ESRL PSD, Boulder, Colorado (available online at http://www.esrl.noaa.gov/psd/). Rain gauges from the Community Collaborative Rain, Hail and Snow Network are available online at https://www.cocorahs.org/. The Weather Research Forecasting model are obtained from University Corporation for Atmospheric Research (available online at https://www2.mmm.ucar.edu/wrf/users/). The authors would like to acknowledge high-performance computing support from Princeton Research Computing.

REFERENCES

Aryal, Y. N., G. Villarini, W. Zhang, and G. A. Vecchi, 2018: Long term changes in flooding and heavy rainfall associated with North Atlantic tropical cyclones: Roles of the North Atlantic Oscillation and El Niño–Southern Oscillation. *J. Hydrol.*, **559**, 698–710, https://doi.org/10.1016/j.jhydrol.2018.02.072.

Atallah, E. H., and L. F. Bosart, 2003: The extratropical transition and precipitation distribution of Hurricane Floyd (1999). *Mon. Wea. Rev.*, **131**, 1063–1081, https://doi.org/10.1175/1520-0493(2003)131<1063:TETAPD>2.0.CO;2.

——, ——, and A. R. Aiyyer, 2007: Precipitation distribution associated with landfalling tropical cyclones over the eastern United States. *Mon. Wea. Rev.*, **135**, 2185–2206, https://doi.org/10.1175/MWR3382.1.

Barlow, M., 2011: Influence of hurricane-related activity on North American extreme precipitation. *Geophys. Res. Lett.*, **38**, L04705, https://doi.org/10.1029/2010GL046258.

Bloemendaal, N., I. D. Haigh, H. de Moel, S. Muis, R. J. Haarsma, and J. C. J. H. Aerts, 2020: Generation of a global synthetic tropical cyclone hazard dataset using STORM. *Sci. Data*, **7**, 40, https://doi.org/10.1038/s41597-020-0381-2.

Caldwell, R. J., J. F. England Jr, and V. L. Sankovich, 2011: Application of radar-rainfall estimates to probable maximum precipitation in the Carolinas. Flood Hydrology and Emergency Management Group Tech. Rep., 94 pp. https://www.researchgate.net/publication/258462881_Application_of_Radar-Rainfall_Estimates_to_Probable_Maximum_Precipitation_in_the_Carolinas.

Chavas, D. R., and K. A. Emanuel, 2010: A QuikSCAT climatology of tropical cyclone size. *Geophys. Res. Lett.*, **37**, L18816, https://doi.org/10.1029/2010GL044558.

Chen, S. S., J. A. Knaff, and F. D. Marks, 2006: Effects of vertical wind shear and storm motion on tropical cyclone rainfall asymmetries deduced from TRMM. *Mon. Wea. Rev.*, **134**, 3190–3208, https://doi.org/10.1175/MWR3245.1.

Chen, X., M. Kumar, and B. L. McGlynn, 2015: Variations in streamflow response to large hurricane-season storms in a southeastern U.S. watershed. *J. Hydrometeor.*, **16**, 55–69, https://doi.org/10.1175/JHM-D-14-0044.1.

Cifelli, R., N. Doesken, P. Kennedy, L. D. Carey, S. A. Rutledge, C. Gimmestad, and T. Depue, 2005: The Community Collaborative Rain, Hail, and Snow Network: Informal education for scientists and citizens. *Bull. Amer. Meteor. Soc.*, **86**, 1069–1078, https://doi.org/10.1175/BAMS-86-8-1069.

Colle, B. A., 2003: Numerical simulations of the extratropical transition of Floyd (1999): Structural evolution and responsible mechanisms for the heavy rainfall over the northeast United States. *Mon. Wea. Rev.*, **131**, 2905–2926, https://doi.org/10.1175/1520-0493(2003)131<2905:NSOTET>2.0.CO;2.

Compo, G. P., and Coauthors, 2015. NOAA/CIRES Twentieth Century Global Reanalysis version 2c.: Research Data Archive at the National Center for Atmospheric Research,

Computational and Information Systems Laboratory, https://doi.org/10.5065/D6N877TW.

Evans, J. L., and R. E. Hart, 2003: Objective indicators of the life cycle evolution of extratropical transition for Atlantic tropical cyclones. *Mon. Wea. Rev.*, **131**, 909–925, https://doi.org/10.1175/1520-0493(2003)131<0909:OIOTLC>2.0.CO;2.

Houze, R. A., 2010: Clouds in tropical cyclones. *Mon. Wea. Rev.*, **138**, 293–344, https://doi.org/10.1175/2009MWR2989.1.

Jiang, H., and E. J. Zipser, 2010: Contribution of tropical cyclones to the global precipitation from eight seasons of TRMM data: Regional, seasonal, and interannual variations. *J. Climate*, **23**, 1526–1543, https://doi.org/10.1175/2009JCLI3303.1.

——, J. B. Halverson, and E. J. Zipser, 2008a: Influence of environmental moisture on TRMM-derived tropical cyclone precipitation over land and ocean. *Geophys. Res. Lett.*, **35**, L17806, https://doi.org/10.1029/2008GL034658.

——, ——, and J. Simpson, 2008b: On the differences in storm rainfall from Hurricanes Isidore and Lili. Part I: Satellite observations and rain potential. *Wea. Forecasting*, **23**, 29–43, https://doi.org/10.1175/2007WAF2005096.1.

Jones, S. C., and Coauthors, 2003: The extratropical transition of tropical cyclones: Forecast challenges, current understanding, and future directions. *Wea. Forecasting*, **18**, 1052–1092, https://doi.org/10.1175/1520-0434(2003)018<1052:TETOTC>2.0.CO;2.

Khouakhi, A., G. Villarini, and G. A. Vecchi, 2016: Contribution of tropical cyclones to rainfall at the global scale. *J. Climate*, **30**, 359–372, https://doi.org/10.1175/JCLI-D-16-0298.1.

Knight, D. B., and R. E. Davis, 2007: Climatology of tropical cyclone rainfall in the southeastern United States. *Phys. Geogr.*, **28**, 126–147, https://doi.org/10.2747/0272-3646.28.2.126.

——, and ——, 2009: Contribution of tropical cyclones to extreme rainfall events in the southeastern United States. *J. Geophys. Res.*, **114**, D23102, https://doi.org/10.1029/2009JD012511.

Kobayashi, S., and Coauthors, 2015: The JRA-55 reanalysis: General specifications and basic characteristics. *J. Meteor. Soc. Japan*, **93**, 5–48, https://doi.org/10.2151/jmsj.2015-001.

Konrad, C. E., II, and L. B. Perry, 2010: Relationships between tropical cyclones and heavy rainfall in the Carolina region of the USA. *Int. J. Climatol.*, **30**, 522–534, https://doi.org/10.1002/joc.1894.

Kunkel, K. E., and S. M. Champion, 2019: An assessment of rainfall from Hurricanes Harvey and Florence relative to other extremely wet storms in the United States. *Geophys. Res. Lett.*, **46**, 13 500–13 506, https://doi.org/10.1029/2019GL085034.

Landsea, C. W., and J. L. Franklin, 2013: Atlantic hurricane database uncertainty and presentation of a new database format. *Mon. Wea. Rev.*, **141**, 3576–3592, https://doi.org/10.1175/MWR-D-12-00254.1.

Li, Y., K. K. W. Cheung, and J. C. L. Chan, 2015: Modelling the effects of land–sea contrast on tropical cyclone precipitation under environmental vertical wind shear. *Quart. J. Roy. Meteor. Soc.*, **141**, 396–412, https://doi.org/10.1002/qj.2359.

Lin, Y., and K. E. Mitchell, 2005: The NCEP Stage II/IV hourly precipitation analyses: Development and applications. *19th Conf. on Hydrology*, San Diego, CA, Amer. Meteor. Soc., 1.2, https://ams.confex.com/ams/pdfpapers/83847.pdf.

Liu, M., and J. A. Smith, 2016: Extreme rainfall from landfalling tropical cyclones in the eastern United States: Hurricane Irene (2011). *J. Hydrometeor.*, **17**, 2883–2904, https://doi.org/10.1175/JHM-D-16-0072.1.

——, G. A. Vecchi, J. A. Smith, and H. Murakami, 2018: Projection of landfalling–tropical cyclone rainfall in the eastern United States under anthropogenic warming. *J. Climate*, **31**, 7269–7286, https://doi.org/10.1175/JCLI-D-17-0747.1.

——, ——, ——, and T. R. Knutson, 2019: Causes of large projected increases in hurricane precipitation rates with global warming. *npj Climate Atmos. Sci.*, **2**, 38, https://doi.org/10.1038/s41612-019-0095-3.

Lonfat, M., F. D. Marks, and S. S. Chen, 2004: Precipitation distribution in tropical cyclones using the Tropical Rainfall Measuring Mission (TRMM) Microwave Imager: A global perspective. *Mon. Wea. Rev.*, **132**, 1645–1660, https://doi.org/10.1175/1520-0493(2004)132<1645:PDITCU>2.0.CO;2.

——, R. Rogers, T. Marchok, and F. D. Marks, 2007: A parametric model for predicting hurricane rainfall. *Mon. Wea. Rev.*, **135**, 3086–3097, https://doi.org/10.1175/MWR3433.1.

Marchok, T., R. Rogers, and R. Tuleya, 2007: Validation schemes for tropical cyclone quantitative precipitation forecasts: Evaluation of operational models for U.S. landfalling cases. *Wea. Forecasting*, **22**, 726–746, https://doi.org/10.1175/WAF1024.1.

Marsooli, R., N. Lin, K. Emanuel, and K. Feng, 2019: Climate change exacerbates hurricane flood hazards along US Atlantic and Gulf Coasts in spatially varying patterns. *Nat. Commun.*, **10**, 3785, https://doi.org/10.1038/s41467-019-11755-z.

Mumby, P. J., R. Vitolo, and D. B. Stephenson, 2011: Temporal clustering of tropical cyclones and its ecosystem impacts. *Proc. Natl. Acad. Sci.*, **108**, 17626–17630, https://doi.org/10.1073/pnas.1100436108.

Murakami, H., G. Villarini, G. A. Vecchi, W. Zhang, and R. Gudgel, 2016: Statistical–dynamical seasonal forecast of North Atlantic and U.S. landfalling tropical cyclones using the high-resolution GFDL FLOR coupled model. *Mon. Wea. Rev.*, **144**, 2101–2123, https://doi.org/10.1175/MWR-D-15-0308.1.

Paerl, H. W., N. S. Hall, A. G. Hounshell, R. A. Luettich, K. L. Rossignol, C. L. Osburn, and J. Bales, 2019: Recent increase in catastrophic tropical cyclone flooding in coastal North Carolina, USA: Long-term observations suggest a regime shift. *Sci. Rep.*, **9**, 10620, https://doi.org/10.1038/s41598-019-46928-9.

Powell, S. W., and M. M. Bell, 2018: Near-surface frontogenesis and atmospheric instability along the U.S. East Coast during the extratropical transition of Hurricane Matthew (2016). *Mon. Wea. Rev.*, **147**, 719–732, https://doi.org/10.1175/MWR-D-18-0094.1.

Prat, O. P., and B. R. Nelson, 2012: Precipitation contribution of tropical cyclones in the southeastern United States from 1998 to 2009 using TRMM satellite data. *J. Climate*, **26**, 1047–1062, https://doi.org/10.1175/JCLI-D-11-00736.1.

Roberts, M. J., and Coauthors, 2020: Projected future changes in tropical cyclones using the CMIP6 HighResMIP Multimodel Ensemble. *Geophys. Res. Lett.*, **47**, e2020GL088662, https://doi.org/10.1029/2020GL088662.

Skamarock, W. C., and Coauthors, 2008: A description of the Advanced Research WRF version 3. NCAR Tech. Note NCAR/TN-475+STR, 113 pp., https://doi.org/10.5065/D68S4MVH.

Smith, J. A., G. Villarini, and M. L. Baeck, 2010: Mixture distributions and the hydroclimatology of extreme rainfall and flooding in the eastern United States. *J. Hydrometeor.*, **12**, 294–309, https://doi.org/10.1175/2010JHM1242.1.

——, A. A. Cox, M. L. Baeck, L. Yang, and P. Bates, 2018: Strange floods: The upper tail of flood peaks in the United

States. *Water Resour. Res.*, **54**, 6510–6542, https://doi.org/10.1029/2018WR022539.

Srock, A. F., and L. F. Bosart, 2009: Heavy precipitation associated with southern Appalachian cold-air damming and Carolina coastal frontogenesis in advance of weak landfalling tropical Storm Marco (1990). *Mon. Wea. Rev.*, **137**, 2448–2470, https://doi.org/10.1175/2009MWR2819.1.

Sturdevant-Rees, P., J. A. Smith, J. Morrison, and M. L. Baeck, 2001: Tropical storms and the flood hydrology of the central Appalachians. *Water Resour. Res.*, **37**, 2143–2168, https://doi.org/10.1029/2000WR900310.

Tippett, M. K., S. J. Camargo, and A. H. Sobel, 2010: A Poisson regression index for tropical cyclone genesis and the role of large-scale vorticity in genesis. *J. Climate*, **24**, 2335–2357, https://doi.org/10.1175/2010JCLI3811.1.

Vecchi, G. A., M. Zhao, H. Wang, G. Villarini, A. Rosati, A. Kumar, I. M. Held, and R. Gudgel, 2011: Statistical–dynamical predictions of seasonal North Atlantic hurricane activity. *Mon. Wea. Rev.*, **139**, 1070–1082, https://doi.org/10.1175/2010MWR3499.1.

——, and Coauthors, 2014: On the seasonal forecasting of regional tropical cyclone activity. *J. Climate*, **27**, 7994–8016, https://doi.org/10.1175/JCLI-D-14-00158.1.

Villarini, G., and J. A. Smith, 2010: Flood peak distributions for the eastern United States. *Water Resour. Res.*, **46**, W06504, https://doi.org/10.1029/2009WR008395.

——, G. A. Vecchi, and J. A. Smith, 2010: Modeling the dependence of tropical storm counts in the North Atlantic Basin on climate indices. *Mon. Wea. Rev.*, **138**, 2681–2705, https://doi.org/10.1175/2010MWR3315.1.

——, J. A. Smith, M. L. Baeck, T. Marchok, and G. A. Vecchi, 2011: Characterization of rainfall distribution and flooding associated with US landfalling tropical cyclones: Analyses of Hurricanes Frances, Ivan, and Jeanne (2004). *J. Geophys. Res.*, **116**, D23116, https://doi.org/10.1029/2011JD016175.

——, G. A. Vecchi, and J. A. Smith, 2012: U.S. landfalling and North Atlantic hurricanes: Statistical modeling of their frequencies and ratios. *Mon. Wea. Rev.*, **140**, 44–65, https://doi.org/10.1175/MWR-D-11-00063.1.

——, R. Goska, J. A. Smith, and G. A. Vecchi, 2014: North Atlantic tropical cyclones and U.S. flooding. *Bull. Amer. Meteor. Soc.*, **95**, 1381–1388, https://doi.org/10.1175/BAMS-D-13-00060.1.

Ware, R. H., and Coauthors, 2000: SuomiNet: A real-time national GPS network for atmospheric research and education. *Bull. Amer. Meteor. Soc.*, **81**, 677–694, https://doi.org/10.1175/1520-0477(2000)081<0677:SARNGN>2.3.CO;2.

Wright, D. B., T. R. Knutson, and J. A. Smith, 2015: Regional climate model projections of rainfall from U.S. landfalling tropical cyclones. *Climate Dyn.*, **45**, 3365–3379, https://doi.org/10.1007/s00382-015-2544-y.

Yang, L., J. Smith, M. Liu, and M. L. Baeck, 2019a: Extreme rainfall from Hurricane Harvey (2017): Empirical intercomparisons of WRF simulations and polarimetric radar fields. *Atmos. Res.*, **223**, 114–131, https://doi.org/10.1016/j.atmosres.2019.03.004.

——, L. Wang, X. Li, and J. Gao, 2019b: On the flood peak distributions over China. *Hydrol. Earth Syst. Sci.*, **23**, 5133–5149, https://doi.org/10.5194/hess-23-5133-2019.

——, and Coauthors, 2020: Riverine flooding and landfalling tropical cyclones over China. *Earth's Future*, **8**, e2019EF001451, https://doi.org/10.1029/2019EF001451.

Zhang, W., G. Villarini, G. A. Vecchi, and J. A. Smith, 2018: Urbanization exacerbated the rainfall and flooding caused by Hurricane Harvey in Houston. *Nature*, **563**, 384–388, https://doi.org/10.1038/s41586-018-0676-z.